


RESEARCH ARTICLE

O₂ permeability of additively manufactured silicone membranes

Marcel Gort¹  | Elodie Morlec² | Damian Gwerder³ | Philipp Schuetz³ | Martin Camenzind² | Mirko Meboldt¹

¹Product Development Group Zurich, Department of Mechanical and Process Engineering, ETH Zurich, Zurich, Switzerland

²Laboratory for Biomimetic Membranes and Textiles, Empa, St. Gallen, Switzerland

³School of Engineering and Architecture, Lucerne University of Applied Sciences and Arts, Horw, Switzerland

Correspondence

Mirko Meboldt, Product Development Group Zurich, Department of Mechanical and Process Engineering, ETH Zurich, Zurich, Switzerland.

Email: meboldtm@ethz.ch

Abstract

Silicone is already widely used in biomedical applications thanks to its outstanding properties. Now additive manufacturing (AM) of silicone can achieve submillimeter details and is offered by SpectroPlast AG as a service. AM of silicone is particularly interesting for designs with complex internal structures such as bioreactors or oxygenators where oxygen permeability is important. Therefore, the oxygen permeability of additively manufactured silicone membranes made from TrueSil (SpectroPlast AG) is studied. Measurements are performed with two membrane thicknesses (0.5 and 0.8 mm) and four different Shore hardnesses (20A, 35A, 50A, and 60A) at 15, 20, and 25°C. The oxygen increase due to diffusion through the membrane is recorded in a cup sealed by the membrane. The oxygen permeability decreases with increasing Shore hardness. TrueSil 20A is comparable to ELASTOSIL[®] Film (Wacker Chemie AG) in terms of oxygen permeability. However, there is a percentage difference of approximately 27% between the measured permeability of ELASTOSIL[®] and the data from the supplier. Membrane thickness does not affect permeability, but the Shore hardness affects the thickness. Membranes with Shore hardness 20A or 35A are manufactured over 0.1 mm thicker than designed, while for Shore hardness 50A and 60A the deviation from the design is less than 0.04 mm.

KEYWORDS

3D-printing, additive manufacturing, O₂ permeability, polydimethylsiloxane (PDMS), silicone

1 | INTRODUCTION

Silicone is used in a wide range of biomedical applications due to its unique properties such as high flexibility, chemical resistance, hydrophobicity, ease of sterilization, biocompatibility, and high gas permeability.^{1–4} Thanks to the progress in material formulation and manufacturing,

additive manufacturing (AM) of silicone is becoming increasingly accessible (e.g., SpectroPlast AG, Schlieren, Switzerland; Elkem ASA, Oslo, Norway; Sterne, Cavaillon, France; innovatiQ GmbH + Co KG, Feldkirchen, Germany). AM of silicone has a big potential in biomedical applications which require complex internal structures such as bioreactors or oxygenators.^{5,6} In these applications,

This is an open access article under the terms of the [Creative Commons Attribution](https://creativecommons.org/licenses/by/4.0/) License, which permits use, distribution and reproduction in any medium, provided the original work is properly cited.

© 2023 ETH Zurich, Lucerne University of Applied Sciences and Arts and Empa, Swiss Federal Laboratories for Materials Science and Technology. *Journal of Applied Polymer Science* published by Wiley Periodicals LLC.

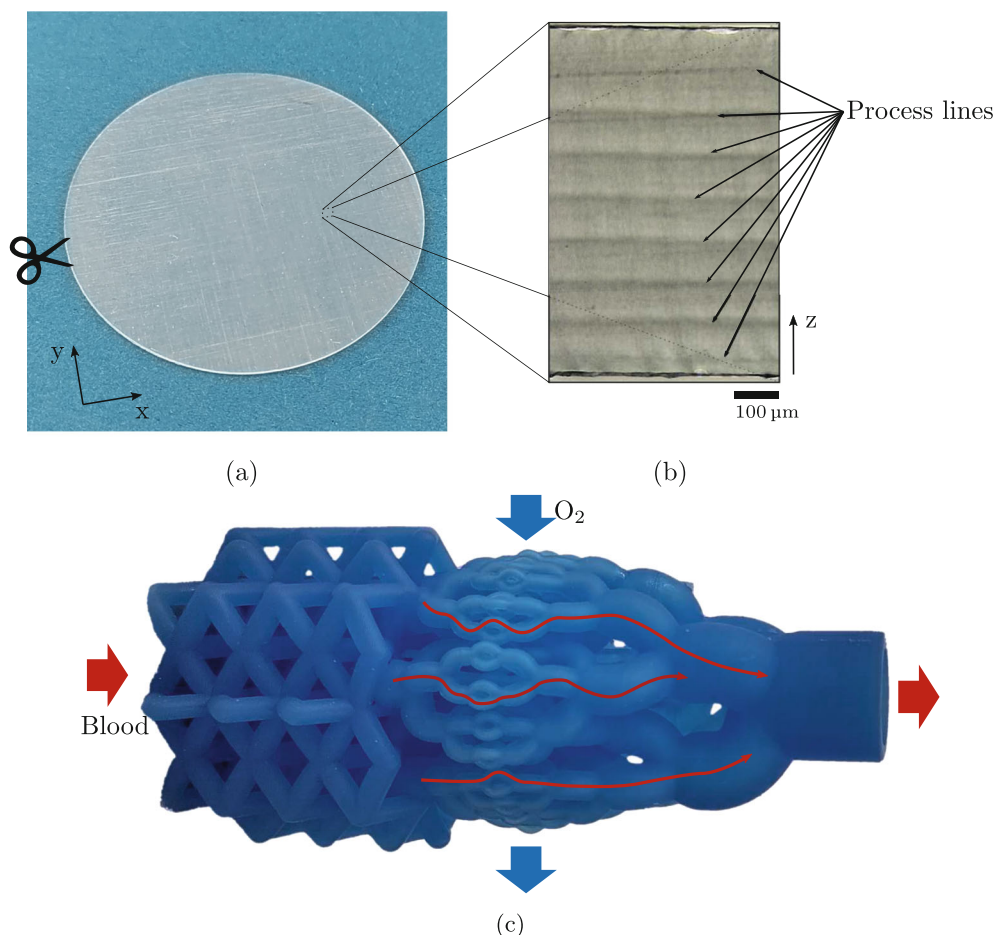


FIGURE 1 (a) Photo of an additively manufactured membrane (0.5 mm, 20A) and (b) cross-section of a membrane (0.8 mm, 60A). (c) Additively manufactured silicone oxygenator prototype made of TrueSil 25A. [Color figure can be viewed at [wileyonlinelibrary.com](https://onlinelibrary.wiley.com/doi/10.1002/app.54079)]

gas exchange and particularly oxygenation are often critical. SpectroPlast AG offers AM of silicone as a service achieving submillimeter spatial resolution and visibly smooth surfaces but the oxygen permeability of the additively manufactured silicone has not yet been characterized. The objective of this study is therefore to determine the oxygen permeability of additively manufactured silicone for the range of Shore hardnesses offered by SpectroPlast.

AM enables complex parts to be fabricated from silicone.^{7–10} One application where AM of silicone has a big potential is fluid handling systems for body fluids such as blood, for example, extracorporeal blood oxygenators or hemodialysis machines.⁶ Figure 1c shows a conceptual additively manufactured silicone oxygenator manufactured in-house using material from SpectroPlast. In addition, bioreactors for cell growth could be printed in silicone to integrate several functions in one part, for example, perfusion, gas exchange, and mechanical stimulation. Several such bioreactors have previously been demonstrated, which have been fabricated using photolithography and casting.^{11–14} Silicone AM promises to simplify the manufacturing process of these bioreactors, reduce the part count, and as a result, reduce the number of interfaces and materials. Each interface of a fluid system is a weak spot, where its failure can

lead to catastrophic consequences such as leakage or contamination. The use of AM allows to increase the system integration, hence, reducing the number of interfaces.⁶ Another advantage of AM for body fluid handling systems is the increased design freedom compared to alternative manufacturing methods which makes it possible to manufacture more physiological channels. One way to exploit the added design freedom is to improve hemocompatibility by geometrically optimizing channels for blood transport, for example, in extra-corporeal blood oxygenators (ECMO).

SpectroPlast has developed TrueSil, a UV-curable silicone optimized for AM with digital light processing (DLP). In DLP, liquid photopolymer resins are polymerized layer by layer with a UV light projector to build a part.¹⁵ The three main process parameters of DLP are layer thickness, light intensity, and exposure time. With increasing membrane thickness the number of layers increases. Two different membrane thicknesses are studied to investigate if a potential difference in diffusivity between inter- and intra-layers causes permeability to change with thickness. Furthermore, all four Shore hardness offered by Spectroplast (20A, 35A, 50A, and 60A) will be compared as Shore hardness positively correlates with density and crosslinking¹⁶ and, hence, is also expected to affect the permeability as previously described.¹⁷ Understanding the influence of

thickness and Shore hardness on the permeability will be valuable to design biomedical devices with TrueSil silicones.

The method chosen for this study determines the permeability from transient state measurements. An additively manufactured sample membrane seals a cup that is initially flushed with nitrogen. During the measurement, the raise in oxygen partial pressure related to the permeation through the membrane from the environment is monitored inside the cup. To investigate the influence of the manufacturing process and the material properties on the permeability, membranes of two different thicknesses and four different Shore hardnesses were used. Further, the measurements were run at three different temperatures to determine the temperature dependency. Gas transport through solid nonporous silicone membranes can be modeled as a solution-diffusion process.¹⁸ The gas permeates from the high-pressure side where it is absorbed into the membrane through molecular diffusion towards the low-pressure side where the gas is released out of the membrane.¹⁹

2 | METHODS

2.1 | Materials

TrueSil 20A, 35A, 50A, and 60A from Spectroplast AG (Schlieren, Switzerland) are investigated. Table 1 summarizes the most important material properties of TrueSil. As reference material, this study uses membranes out of ELASTOSIL® Film 2030 250/200 (Wacker Chemie AG, Munich, Germany) with a thickness of 0.20 mm and a permeability of 484Barrer (20°C,

30 µm). Three membranes with a diameter of 54 mm were punched out of the ELASTOSIL® sheet as reference samples.

To evaluate the permeability of TrueSil depending on Shore hardness and thickness, this study analyzed and compared 40 different membrane samples in total. Membranes with a diameter of 60 mm and a thickness of 0.5 mm and 0.8 mm with Shore hardness 20A, 35A, 50A, and 60A were additively manufactured for a total of 8 different types of membrane. Five samples of each type of membrane were manufactured by SpectroPlast AG. Each membrane was printed separately. After printing, the membranes were punched out to a diameter of 54 mm removing thinning effects towards the edge of the membranes. The membranes were separately stored in labeled zip bags between experiments and handled with gloves to prevent moisture and dirt from attaching to their surface. Figure 1a shows an additively manufactured membrane. Additionally, the cross-section of a membrane is depicted in Figure 1b.

The thickness of each membrane was determined with an industrial CT scanner (Diondo D2, Diondo GmbH, Hattingen, Germany). Ten membranes were stacked with an air gap of approximately 4 mm and measured at the same time. Volumegraphics Studio MAX (Volume Graphics GmbH, Heidelberg, Germany) was used to process and analyze the CT data. Within Volumegraphics Studio MAX the ray method was used to determine the thickness of the membranes.

2.2 | Design of experiment

In total 120 measurements were taken in three blocks of 40 measurements with temperature as the blocking factor. The order of temperature blocks was 25, 15, and 20°C. There were 5 samples for each combination of thickness and Shore hardness ($n = 5$). Within the blocks the sequence of the measurements was randomized. Twelve measurements were taken with the reference membranes subdivided into four temperature blocks of 25, 15, 20, and 0°C. The factors and levels for both experiments with TrueSil and ELASTOSIL® are summarized in Table 2.

TABLE 1 Material properties of TrueSil from Spectroplast AG.

Property	Shore hardness			
	20A	35A	50A	60A
Tensile strength	4.9 MPa	5.5 MPa	7.3 MPa	8.5 MPa
Elongation at break	1000%	650%	530%	360%
Tear strength	5.8 $\frac{\text{N}}{\text{mm}}$	10 $\frac{\text{N}}{\text{mm}}$	11 $\frac{\text{N}}{\text{mm}}$	17 $\frac{\text{N}}{\text{mm}}$
Density	1.05 $\frac{\text{g}}{\text{cm}^3}$	1.08 $\frac{\text{g}}{\text{cm}^3}$	1.11 $\frac{\text{g}}{\text{cm}^3}$	1.13 $\frac{\text{g}}{\text{cm}^3}$

TABLE 2 Factors and levels for both experiments using TrueSil and ELASTOSIL®.

	Factors		
	Shore hardness (A)	Temperature (°C)	Thickness (mm)
TrueSil			
Levels	20, 35, 50, 60	15, 20, 25	0.5, 0.8
ELASTOSIL®			
Levels	20	0, 15, 20, 25	0.2

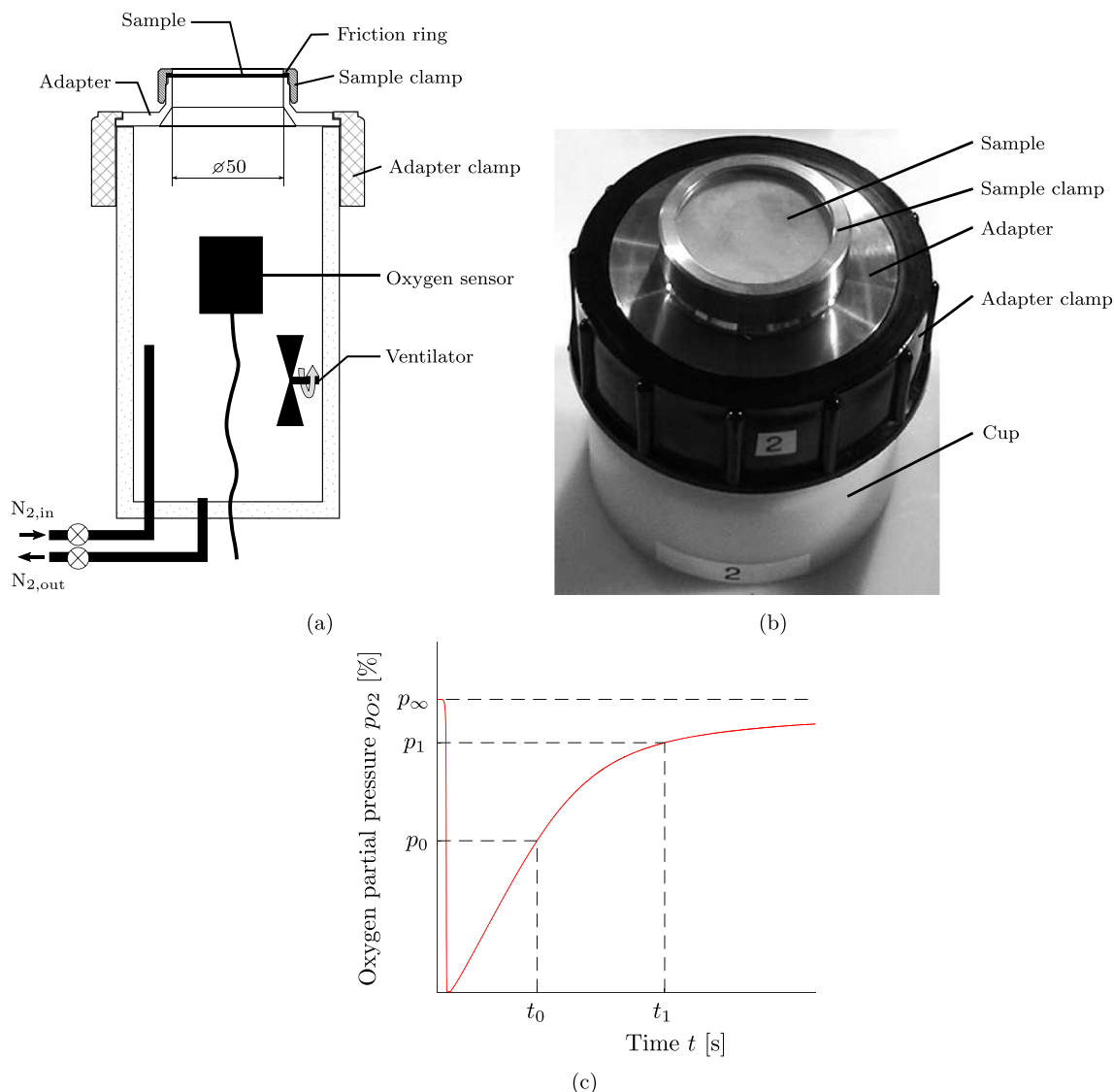


FIGURE 2 (a) Cross-section of the permeability measurement setup, (b) picture of the permeability measurement setup, and (c) exemplary oxygen partial pressure over time. [Color figure can be viewed at [wileyonlinelibrary.com](https://onlinelibrary.wiley.com/doi/10.1002/app.54079)]

2.3 | O₂ permeance measurement

The oxygen permeance of the membranes was measured with the setup shown in Figure 2a. The entire setup was operated inside a climatic chamber in which the temperature and humidity were controlled. Throughout all the measurements the relative humidity was kept constant at 65%. This humidity was chosen to emulate the humidity at which oxygenators are most likely to be operated. The setup consisted of a cup that was sealed on top by the membrane. Installing the membranes consisted of the following steps: first, the membrane was placed on a paper disk. Second, the paper with the membrane was positioned on the membrane adapter. Once the membrane was correctly positioned the paper was removed from underneath the membrane. Finally, a friction ring

was placed on the membrane and the membrane was clamped by tightening the sample clamp.

Once temperature and humidity stabilized around the target, the measurement was started. An electrochemical oxygen sensor (FYA600O2, Ahlborn Mess-und Regelungstechnik GmbH, Germany) monitored the raise of oxygen partial pressure due to permeation through the membrane. The oxygen sensor was calibrated in air (20.95% O₂) before each measurement. A data logger (MSR145, MSR Electronics GmbH, Switzerland) installed next to the setup recorded absolute pressure, relative humidity, and temperature. All data were recorded with a sampling frequency of 0.2 Hz.

At the start of the measurement, the cup was purged with nitrogen until the oxygen level was below 0.1%. During the purging, a ventilator mixed the air within the

cup. After closing the nitrogen supply valve, the purge valve was left open for another 20s to allow the pressure inside the cup to equalize with the environment. The evaluation was started after the oxygen partial pressure reached 0.2% and was terminated 150 min into the measurement.

2.4 | Calculation of O₂ permeability

By the conservation of mass, the change in oxygen inside of the measurement cup $\dot{n}_{O_2, \text{cup}}$ must be equal to the flux of oxygen through the membrane $\dot{n}_{O_2, \text{membrane}}$

$$\dot{n}_{O_2, \text{cup}} = \dot{n}_{O_2, \text{membrane}}. \quad (1)$$

The following assumptions are made: constant atmospheric pressure, constant diffusivity, the oxygen is homogeneously mixed inside of the cup as the diffusion of oxygen in nitrogen is about four orders of magnitude faster than in silicone, and the diffusion of oxygen is decoupled from the diffusion of other gases mainly nitrogen or water vapor. By applying the ideal gas law, the change in oxygen $\dot{n}_{O_2, \text{cup}}$ can be related to the change in partial pressure $\frac{dp_{O_2, \text{cup}}}{dt}$

$$\dot{n}_{O_2, \text{cup}} = \frac{V}{R \cdot T} \cdot \frac{dp_{O_2, \text{cup}}}{dt}, \quad (2)$$

where V is the volume of the gas inside of the measurement cup, R is the universal gas constant, and T is the temperature. According to Fick's first law, the gas flux per unit area J through a membrane is described as

$$J = \frac{P}{\delta} \cdot (p_{O_2, \infty} - p_{O_2, \text{cup}}), \quad (3)$$

where P is the material specific permeability, δ is the membrane thickness and $p_{O_2, \infty}$ and $p_{O_2, \text{cup}}$ are the pressure on the high and low side respectively.¹⁸ Multiplying the gas flux by the area of the membrane A gives the molar flow

$$\dot{n}_{O_2, \text{membrane}} = \frac{A}{\delta} \cdot P \cdot (p_{O_2, \infty} - p_{O_2, \text{cup}}). \quad (4)$$

Inserting Equation (2) and (4) into Equation (1) leads to the following differential Equation

$$\frac{V}{R \cdot T} \cdot \frac{dp_{O_2}}{dt} = \frac{A}{\delta} \cdot P \cdot (p_{O_2, \infty} - p_{O_2, \text{cup}}), \quad (5)$$

which solves to

$$p_{O_2, \text{cup}}(t) = p_{O_2, \infty} - [p_{O_2, \infty} - p_{O_2, \text{cup}}(t=0)] \cdot \exp\left[-\frac{V}{R \cdot T} \cdot \frac{A}{\delta} \cdot P \cdot t\right]. \quad (6)$$

Solving (6) for the permeability P gives

$$P = \frac{\delta}{A} \frac{V}{R \cdot T \cdot \Delta t} \cdot \ln\left(\frac{p_{O_2, \infty} - p_{O_2, \text{cup}}(t_0)}{p_{O_2, \infty} - p_{O_2, \text{cup}}(t_1)}\right), \quad (7)$$

where t_0 and t_1 are start and end times of the evaluation period. Finally, the temperature dependency of the permeability can be described using the Arrhenius equation

$$P = P_0 \cdot \exp\left(\frac{-E_p}{R \cdot T}\right), \quad (8)$$

where P_0 is a constant and E_p is the gas specific activation energy of permeation.¹⁹

3 | RESULTS

Figure 3a summarizes all results from the permeability measurements. The oxygen permeability of TrueSil decreases with increasing Shore hardness. The decrease is most pronounced between Shore hardness 50A and 60A. TrueSil 20A and ELASTOSIL[®] have both a Shore hardness of 20A and the two materials behave similarly in terms of oxygen permeability. The similarity of the two materials is even clearer when considering Figure 3c where the oxygen permeance of ELASTOSIL[®] with a thickness of 0.2 mm is compared to the oxygen permeance of TrueSil 20A with thicknesses between 0.6 and 1 mm. The comparison is done by fitting a function with only the thickness as a variable through all measurements taken at 20°C of ELASTOSIL[®] and TrueSil 20A. The $R^2 > 0.999$ between the fit and the measurements underlines the similarity. The high R^2 together with the data shown in Figure 3a suggest that the thickness of the membranes has no effect on permeability. Within the examined temperature range of 15–25°C, the oxygen permeability of ELASTOSIL[®] and all TrueSil variants increased with increasing temperature.

Measuring the thickness of the 3D-printed membranes revealed a correlation between deviation from the target thickness and the Shore hardness. As shown in Figure 3b, for both thicknesses the positive deviation is the largest for the lowest Shore hardness. With increasing Shore hardness the deviation decreases until it becomes negative for the highest Shore hardness of 60A. For the calculation of

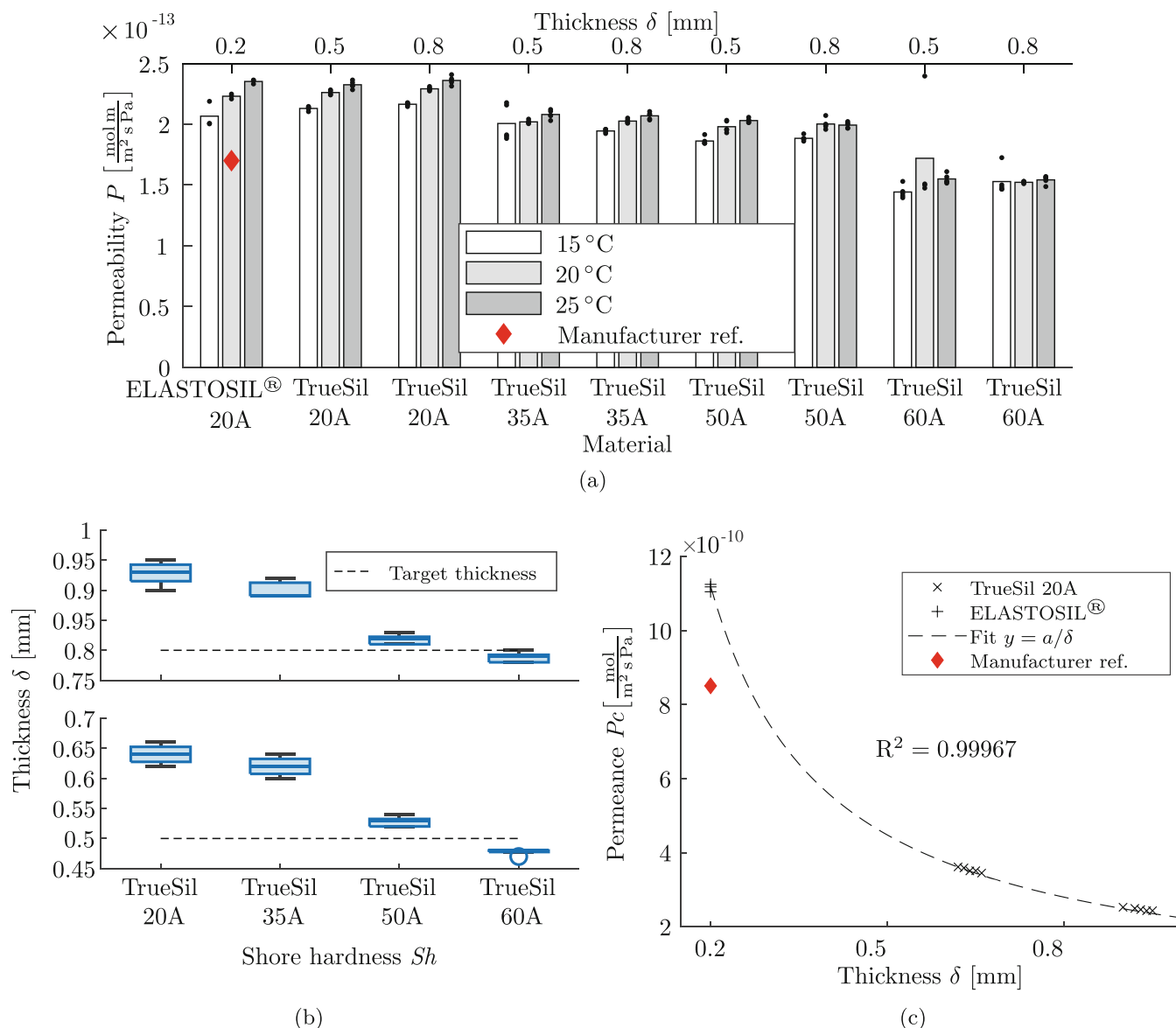


FIGURE 3 Graphical summary of all results starting with (a) the permeability of all measured samples and temperatures, (b) the correlation between thickness δ and Shore hardness Sh of additively manufactured TrueSil membranes, and (c) a comparison of the permeance P_c of TrueSil 20A and ELASTOSIL® (20A) at 20 °C. The linear function fitted through the data points allows comparing the different thicknesses and materials. [Color figure can be viewed at [wileyonlinelibrary.com](https://onlinelibrary.wiley.com/terms-and-conditions)]

permeability, the measured thickness of each membrane was used.

The permeability of ELASTOSIL® measured in this study has a percentage difference of approximately 27% compared to the value provided by Wacker (red diamond in Figure 3c and 3a). Possible reasons for this difference are highlighted in the discussion section.

4 | DISCUSSION

The observed decrease in permeability with increasing Shore hardness is probably linked to the change in the

polymer composition. Interestingly, the oxygen permeability of TrueSil 35A and TrueSil 50A is similar while there is a clear difference between TrueSil 20A and TrueSil 35A as well as TrueSil 50A and TrueSil 60A. This discontinuity of the decrease in permeability between Shore hardness 35A and 50A indicates that there might be other effects at play. From a design perspective, the discontinuity could be exploited when both a higher Shore hardness and oxygen permeability are required.

Gas permeability is governed by several material properties and solvents used during processing.^{19,20} In the case of additively manufactured silicone, some variation in permeability can be expected to arise from post-processing by

varying exposure times to solvents to remove excess material. After washing, the part is finally cured with heat. Variation in temperature or time of the heat treatment is an additional source for variation in material properties. Finally, there also is material batch-related variance. The following subsections discuss the thickness deviation arising from the AM process, the deviation in permeability, and finally outlier handling.

4.1 | Thickness deviation

To further investigate the observed thickness deviation the cross-section of the membranes was studied. Cross-sections were prepared by punching out discs with a diameter of 6 mm from various sections of the membranes. These discs were then embedded in optimal cutting temperature compound and cut into slices of 10 μm on a microtome-cryostat at -20°C . Using a laser scanning microscope (VK-X200K, Keyence International SA, Mechelen, Belgium) the process lines could be visualized as shown in Figure 1b. By measuring the distance between the process lines the thickness of each layer was approximated revealing that the first layer is 140 μm to 160 μm thick instead of the intended layer thickness of 100 μm for Shore hardness 20A and 35A and the last layer also appears to be thicker at around 130 μm for the same Shore hardnesses. Layers in between top and bottom layer are approximately 120, 110, 90–100 μm , and 95 μm for Shore hardness 20A, 35A, 50A, and 60A, respectively. While the top layer of 50A and 60A membranes is thickened too with 160 μm and 120 μm , respectively, the bottom layer is close to the target thickness.

4.2 | Permeability deviation

A percentage difference of approximately 27% is found when comparing the permeability of ELASTOSIL[®] provided by the supplier with the permeability determined in this study. We assume there are three main sources responsible for this difference: (1) different measurement conditions in particular relative humidity, (2) the effect of measuring at transient state, and (3) leakage of the measurement setup.

Oxygen permeability might increase with increasing relative humidity as shown for other polymers.²¹ This study kept the relative humidity at 65%. If the permeability provided by the supplier was measured at lower relative humidity, this would account for some of the difference.

This study used transient state measurements. On the one hand, the test setup is simplified by doing transient state measurements but on the other hand, there are

more unknowns and it is more difficult to model mass transport. For instance, the nitrogen used to purge the cup at the start is dry as a result the relative humidity in the measurement cup drops below 20% during purging to then quickly raise back to above 50% within the 2.5 h of measurement. The water vapor flux might influence the oxygen flux¹⁹ even though the silicone membranes in this study were rubbery. Besides, the change in relative humidity also affects the read-out of the oxygen sensor.

While the first two error sources are difficult to quantify, leakage can be estimated using the same approach as to determine the permeability. The leakage was estimated by measuring the flow of oxygen into the measurement cup while the cup was sealed with a steel plate instead of a membrane. Oxygen entering the cup was considered leakage. Going back to Equation (1) and replacing the gas flow through the membrane with the leak flow gives

$$\dot{n}_{\text{O}_2,\text{cup}} = \dot{n}_{\text{O}_2,\text{leakage}}. \quad (9)$$

Furthermore, assuming molecular flow properties for the leakage leads to

$$\frac{V}{R \cdot T} \cdot \frac{dp}{dt} = L \cdot \sqrt{\frac{T}{M_{\text{O}_2}}} \cdot (p_{\text{O}_2,\infty} - p_{\text{O}_2,\text{cup}}), \quad (10)$$

where L and M_{O_2} are the leakage factor and molecular weight of oxygen respectively, which solves to

$$L = \frac{V}{R \cdot T \cdot \Delta t} \cdot \sqrt{\frac{M_{\text{O}_2}}{T}} \cdot \ln \left(\frac{p_{\text{O}_2,\infty} - p_{\text{O}_2,\text{cup}}(t_0)}{p_{\text{O}_2,\infty} - p_{\text{O}_2,\text{cup}}(t_1)} \right). \quad (11)$$

Using Equation (11) results in a leakage factor of $L = 2.07 \times 10^{-14} \text{ mols}^{-1} \text{ Pa}^{-1}$. Table 3 summarizes the effect of leakage on the permeability measurement for various measurement conditions. Thereafter, leakage accounts for approximately 12% of the total difference between the permeability provided by the supplier and this study.

TABLE 3 Effect of leakage on permeability in $10^{-14} \left[\frac{\text{mol m}}{\text{m}^2 \text{ s Pa}} \right]$ for the different membrane thicknesses and temperature blocks.

Temperature (T)	Thickness δ		
	0.2 mm	0.5 mm	0.8 mm
15°C	0.63	1.59	2.54
20°C	0.64	1.60	2.56
25°C	0.65	1.61	2.58

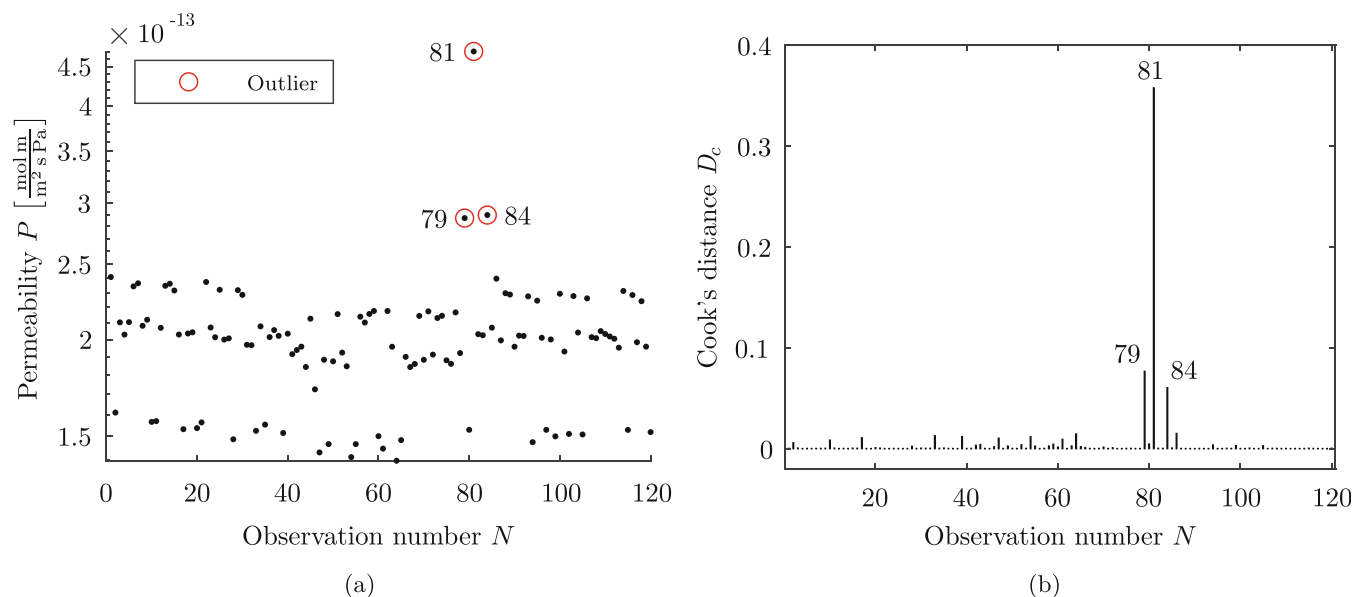


FIGURE 4 Both plots (a) showing the permeability (logarithmic scale) measured for all samples and conditions and (b) showing Cook's distance when fitting a linear model of the form described in Equation (12) indicate that observation 79, 81, and 84 are outliers. Observations 79, 81, and 84 correspond to the following conditions: thickness 0.8 mm, Shore hardness 35A at 15°C; thickness 0.5 mm, Shore hardness 60A at 20°C; thickness 0.8 mm, Shore hardness 60A at 20°C. [Color figure can be viewed at [wileyonlinelibrary.com](https://onlinelibrary.wiley.com/doi/10.1002/app.54079)]

4.3 | Outliers

Observations 79, 81, and 84 were removed from the final evaluation because they are assumed to be outliers. This assumption is supported by Figure 4a where observations 79, 81, and 84 are considerably above all other observations of the same samples at different temperatures or of similar samples at the same temperature. Finally, the above observations also are obvious outliers when calculating Cook's distance as shown in Figure 4b. The linear model used to calculate Cook's distance is of the form

$$\text{Permeability} \sim \text{ShoreHardness} \cdot \text{Temperature} \cdot \text{Thickness.} \quad (12)$$

The thickness is only included in the model due to the deviation from the target thickness. Furthermore, observations 79, 81, and 84 were taken at 15, 20, and 20°C, respectively. Measurements of the same samples at 25°C (observations 3, 33, and 28, respectively) resulted in a lower permeability which violates the assumption that permeability increases with temperature while the rest of the data confirms the same assumption. Hence, we assume that these outliers are caused by a faulty installation of the membrane which increases the leakage.

In Figure 3a one can find more observations which could be labeled as outliers (e.g. one observation of TrueSil 60A with a thickness of 0.5 mm at 20°C). However,

these observations are only significantly different compared to observations with the same Shore hardness. We decided to keep these “local” outliers to avoid the risk of distorting the results.

5 | CONCLUSION

Additively manufactured TrueSil membranes have a comparable oxygen permeability to ELASTOSIL® and other silicones.^{19,22} As temperature increases, the oxygen permeability of TrueSil increases. The higher the Shore hardness of TrueSil, the lower the permeability. No significant difference in permeability between 0.5 and 0.8 mm thick membranes could be found. However, we found a correlation between the Shore hardness and the thickness of additively manufactured membranes where softer membranes would deviate more from the design thickness.

Silicone additive manufacturing is enabling entirely new designs in biomedical devices. Knowledge of the relationships between permeability and shore hardness, as well as shore hardness and thickness, will aid the design process. When gas permeability and Shore hardness are both relevant parameters one should carefully consider the nonlinear relationship between the two parameters.

In the present study, the membranes were exclusively manufactured flat with the thickness in the printing direction. Membranes manufactured vertically are needed to further investigate the influence of the membrane of the

print direction on the oxygen permeability. Finally, the presented measurement setup offers good precision, but its accuracy must be examined.

AUTHOR CONTRIBUTIONS

Marcel Gort: Conceptualization (equal); data curation (lead); formal analysis (lead); investigation (supporting); methodology (lead); project administration (lead); software (lead); validation (lead); visualization (lead); writing – original draft (lead); writing – review and editing (lead). **Elodie Morlec:** Investigation (lead); methodology (supporting); resources (supporting); writing – review and editing (supporting). **Damian Gwerder:** Formal analysis (supporting); investigation (supporting); methodology (supporting); writing – review and editing (supporting). **Philipp Schuetz:** Conceptualization (supporting); resources (supporting); supervision (supporting); writing – review and editing (supporting). **Martin Camenzind:** Conceptualization (equal); formal analysis (supporting); investigation (supporting); methodology (supporting); resources (equal). **Mirko Meboldt:** Conceptualization (supporting); formal analysis (supporting); funding acquisition (lead); project administration (supporting); resources (equal); supervision (lead); writing – review and editing (equal).

ACKNOWLEDGMENTS

The authors would like to thank SpectroPlast AG and Wacker Chemie AG for providing the samples for the present study. Open access funding provided by Eidgenossische Technische Hochschule Zurich.

FUNDING INFORMATION

This research received no specific grant from any funding agency in the public, commercial, or not-for-profit sectors. Material samples by SpectroPlast AG and Wacker Chemie AG have been provided for free.

DATA AVAILABILITY STATEMENT

Data that support the findings of this study are available from the corresponding author upon reasonable request.

ORCID

Marcel Gort  <https://orcid.org/0000-0001-9998-1619>

REFERENCES

- [1] V. R. Sastri, *Plastics in Medical Devices*, 3rd Ed., William Andrew Publishing, Norwich, NY **2022**.
- [2] J. N. Lee, C. Park, G. M. Whitesides, *Anal. Chem.* **2003**, 75, 6544.
- [3] J. A. Smith, S. Li, E. Mele, A. Goulas, D. Engström, V. V. Silberschmidt, *J. Mech. Behav. Biomed. Mater.* **2021**, 115, 104291.
- [4] W. Qian, X. Hu, W. He, R. Zhan, M. Liu, D. Zhou, Y. Huang, X. Hu, Z. Wang, G. Fei, J. Wu, M. Xing, H. Xia, G. Luo, *Colloids Surf., B* **2018**, 166, 61.
- [5] F. Liravi, E. Toyserkani, *Addit. Manuf.* **2018**, 24, 232.
- [6] C. Zhang, S. Wang, J. Li, Y. Zhu, T. Peng, H. Yang, *Addit. Manuf.* **2020**, 36, 101490.
- [7] F. B. Coulter, M. Schaffner, J. A. Faber, A. Rafsanjani, R. Smith, H. Appa, P. Zilla, D. Bezuidenhout, A. R. Studart, *Material* **2019**, 1, 266.
- [8] N. Bhattacharjee, C. Parra-Cabrera, Y. T. Kim, A. P. Kuo, A. Folch, *Adv. Mater.* **2018**, 30, 1800001.
- [9] M. Zare, E. R. Ghomi, P. D. Venkatraman, S. Ramakrishna, *J. Appl. Polym. Sci.* **2021**, 138, 50969.
- [10] E. Fleck, A. Sunshine, E. DeNatale, C. Keck, A. McCann, J. Potkay, *Micromachines* **2021**, 12, 1266.
- [11] S. K. Sia, G. M. Whitesides, *Electrophoresis* **2003**, 24, 3563.
- [12] R. Koens, Y. Tabata, J. C. Serrano, S. Aratake, D. Yoshino, R. D. Kamm, K. Funamoto, *APL Bioeng.* **2020**, 4, 16106.
- [13] J. Liu, H. Zheng, X. Dai, P. S. P. Poh, H.-G. Machens, A. F. Schilling, *Front. Bioeng. Biotechnol.* **2020**, 8, 568934.
- [14] N. Mori, Y. Morimoto, S. Takeuchi, *Biofabrication* **2018**, 11, 11001.
- [15] A. Davoudinejad, *Additive Manufacturing*, Elsevier, Amsterdam, the Netherlands **2021**, p. 159.
- [16] J. Kuncova-Kallio, P. J. Kallio. International Conference of the IEEE Engineering in Medicine and Biology Society. IEEE, New York, NY, 2486–2489. **2006**.
- [17] A. Lamberti, S. L. Marasso, M. Cocuzza, *RSC Adv.* **2014**, 4, 61415.
- [18] J. Wijmans, R. Baker, *J. Membr. Sci.* **1995**, 107, 1.
- [19] J. E. Mark Ed., *Physical Properties of Polymers Handbook*, 2nd ed., Springer, New York **2006**.
- [20] H. Lin, T. Kai, B. D. Freeman, S. Kalakkunnath, D. S. Kalika, *Macromolecules* **2005**, 38, 8381.
- [21] J. Catalano, T. Myezwa, M. De Angelis, M. G. Baschetti, G. Sarti, *Int. J. Hydrogen Energy* **2012**, 37, 6308.
- [22] S. C. Fraga, M. A. Azevedo, I. M. Coelho, C. Brazinha, J. G. Crespo, *Sep. Purif. Technol.* **2018**, 197, 18.

SUPPORTING INFORMATION

Additional supporting information can be found online in the Supporting Information section at the end of this article.

How to cite this article: M. Gort, E. Morlec, D. Gwerder, P. Schuetz, M. Camenzind, M. Meboldt, *J. Appl. Polym. Sci.* **2023**, 140(30), e54079. <https://doi.org/10.1002/app.54079>